Available online at www.sciencedirect.com
ScienceDirect
Ceramics International 36 (2010) 2431–2439
CERAMICS INTERNATIONAL
www.elsevier.com/locate/ceramint

Development of macroporous nanocomposite scaffolds of gelatin/bioactive glass prepared through layer solvent casting combined with lamination technique for bone tissue engineering

Masoud Mozafari [a,*], Fathollah Moztarzadeh [a], Mohammad Rabiee [a], Mahmoud Azami [a], Saied Maleknia [a], Mohammadreza Tahriri [a], Zoha Moztarzadeh [b], Nader Nezafati [a]

[a] *Biomaterials Group, Faculty of Biomedical Engineering (Center of Excellence), Amirkabir University of Technology, P.O. Box 15875-4413, Tehran, Iran*
[b] *Institute of Bioinformatic, Münster University, Münster, Germany*

Received 17 December 2009; received in revised form 30 April 2010; accepted 30 June 2010
Available online 3 August 2010

Abstract

In this study, macroporous bioactive nanocomposite scaffolds were developed using cross-linked gelatin and bioactive glass (BaG) nanoparticles. First, BaG nanoparticles were synthesized via sol–gel method and characterized. Then, macroporous nanocomposites were prepared through layer solvent casting combined with freeze-drying and lamination techniques. This research has developed a new composition to produce a new bioactive nanocomposite which is porous with three-dimensional (3D) inter-connected microstructure, pore sizes are 200–500 μm, porosity are 72–86% and BaG nanoparticles are dispersed evenly among cross-linked gelatin matrices. It is mentionable that in this study, we have reported the formation of chemical bonds between BaG nanoparticles and gelatin for the first time. Finally, the *in vitro* cytocompatibility of the nanocomposite scaffolds was tested using SaOS-2 cell line.

Keywords: A. Sol–gel processes; B. Nanocomposites; B. Porosity; D. Glass; E. Biomedical applications

1. Introduction

In the past few years, increasing attention has been paid to nanocomposites made of biopolymers and bioactive materials for application in tissue engineering [1–4]. A wide variety of nanocomposites are currently being explored for use as porous scaffolds for many tissue engineering strategies. Nanocomposite scaffolds may prove necessity for reconstruction of multi-tissue organs, tissues interfaces, and structural tissue including bone, cartilage, tendons, ligaments and muscles [5].

The aim of creating nanocomposites is to have a nanoscale interaction between the bioactive inorganic phase and the organic phase, creating a tough material. This intimate interaction should allow bone cells to come into contact with both phases at one time, and the material should degrade at a single rate. Nanocomposites can be divided into two classes. One is a nanoscale version of a conventional composite, where nanoparticles are dispersed in a polymer matrix. The second is where the inorganic and organic phases are chemically bonded together at a molecular scale during processing. These materials are termed hybrids here and have the greatest potential of combining the desired properties of the constituent materials for bone regeneration [6,7]. In addition, the construct should possess mechanical properties similar to the surrounding host tissue in order to provide structural stability to a defect site without absorbing all of the mechanical stresses, which would result in stress shielding of the natural tissue and its eventual resorption. Furthermore, as the scaffold serves only as temporary support until bone is formed within the defect site, the ability to breakdown gradually into nontoxic degradation products either through hydrolysis or enzymatic degradation is also important [8,9]. Many kind of bioactive materials including bioactive glasses, bioactive glass–ceramics, and calcium phosphate ceramics, have been developed and some of them are now applied to repair and reconstruct diseased or damaged bones or tissues. Bioactive glasses meet the first three

* Corresponding author. Tel.: +98 21 22373717; fax: +98 21 22354162.
E-mail address: mmozafari@aut.ac.ir (M. Mozafari).

0272-8842/$36.00
doi:10.1016/j.ceramint.2010.07.010

criteria: excellent osteoconductivity and bioactivity, ability to deliver cells, and controllable biodegradability. These advantages make bioactive glasses promising scaffold materials for tissue engineering [10].

In this case, using gelatin as a biodegradable biopolymer and BaG nanoparticles as bioactive material to create a scaffold with biodegradability, bioactivity, high porosity, suitable mechanical properties and toughness is really suitable. Gelatin is a natural polymer derived from collagen by hydrolysis and has almost identical composition as that of collagen [11]. Since gelatin is a denatured biopolymer, the selection of gelatin as a scaffolding material can circumvent the concerns of immunogenicity and pathogen transmission associated with collagen [12]. However, it has poor mechanical property. Therefore, a porous gelatin scaffold can be used as bone substitute for bone repair and reconstruction only if its mechanical property can be improved with addition of biomaterials like hydroxyapatite, aluminosilicate (geopolymers), BaG ceramic, etc. Several methods have been used to produce porous three-dimensional scaffolds, including biopolymers replication [13–16], sintering (thermal bonding) a porous mass of particles [17] or fibers [18,19], the use of foaming agents [20], solid freeform fabrication [21], sol–gel [22] and freeze-drying methods [23,24] but porous gelatin scaffolds can be fabricated by using the freeze-drying method as an effective method. Just as in the production of polymer scaffolds, for this scaffold, factors such as gelatin solution concentration, bioactive glass type and size, freeze-drying parameters, etc. play very important roles in forming the scaffolds of desired porous structures and hence the mechanical performance [25].

There is a growing interest in the use of BaG in scaffolds for bone repair [26,27]. BaG has a widely recognized ability to foster the growth of bone cells [28,29], and to bond strongly with hard and soft tissue [30]. Upon implantation, BaG undergoes specific reactions, leading to the formation of a hydroxyl carbonate apatite (HCA) layer, amorphous calcium phosphate (ACP) or crystalline hydroxyapatite (HA) phase on the surface of the bioactive glass, which is responsible for their strong bonding with surrounding tissue [31]. A gel-derived glass with as much as 80 mol% SiO_2 develops a hydroxyl carbonate apatite (HCA) layer in a short time when in contact with physiological solutions like SBF, whereas melt-glass with less than 55 mol% SiO_2 requires several days to form a polycrystalline HCA layer [31]. This high reactivity of sol–gel derived glasses is related to a larger volume fraction of nanometer porosity on surface, larger concentration of silanols on the surface [32] and higher surface area [33] than those of melt-derived glasses.

In this study, we synthesized using the sol–gel method, a new bioactive glass in the ternary system SiO_2–CaO–P_2O_5 named 64S. Its molar composition 64%SiO_2–31%CaO–5%P_2O_5 is enriched in phosphorous oxide at the expense of calcium oxide. Then, to mimic the mineral and organic component of natural bone, the BaG and gelatin nanocomposite was prepared via layer solvent casting combined with freeze-drying and lamination techniques. Finally, glutaraldehyde (GA) was used as a cross-linking agent. The methodologies used for the synthesizing of the nanocomposite were described and also in this research, we have reported formation of chemical bonds between BaG nanoparticles and gelatin. Eventually, the cellular responses of the bioactive scaffolds were examined.

2. Materials and methods

2.1. Materials

Tetraethylorthosilicate (TEOS: $C_8H_{20}O_4Si$), calcium nitrate ($Ca(NO_3)_2{\cdot}4H_2O$), and triethyl phosphate (TEP: $C_6H_{15}O_4P$) and 0.1 M nitric acid (HNO_3), were purchased from Merck Inc. The gelatin used in this research was purchased from Merck (microbiology grade, No. 107040) at 10% (w/v) concentration. Also, GA ($C_5H_8O_2$) solution of 1% (w/v) was purchased from Merck Inc.

2.2. Synthesis of BaG nanopowder

The sol–gel-prepared glass materials SiO_2–P_2O_5–CaO (64%SiO_2, 5%P_2O_5, and 31%CaO) (based on mol%), was synthesized and characterized. The solution for the glass was prepared and described as follows: 14.8 g (0.064 mol) of tetraethoxysilane was added into 30 mL of 0.1 M nitric acid, the mixture was allowed to react for 30 min for the acid hydrolysis of TEOS to proceed almost to completion. The following reagents were added in sequence allowing 45 min for each reagent to react completely: 0.85 g (0.005 mol) triethylphosphate, and 7.75 g (0.031 mol) of calcium nitrate tetrahydrate. After the final addition, mixing was continued for 1 h to allow completion of the hydrolysis reaction. The solution was cast in a cylindrical Teflon container and kept sealed for 10 days at room temperature to allow the hydrolysis and a polycondensation reaction to take place until the gel was formed. The gel was kept in a sealed container and heated at 70 °C for an additional 3 days. The water was removed and a small hole was inserted in the lid to allow the leakage of gases while heating the gel to 120 °C for 2 days to remove all the water. Subsequently, the powders were milled by planetary milling (SVD15IG5-1, LG Company) with 400 rpm during 10 h. After grinding and sieving, the dry powder heated 24 h at 700 °C for nitrate elimination. Finally the powder was ground for 10 h for achieving BaG nanoparticles.

2.3. Preparation of nanocomposite samples

The preparation process of these scaffolds is shown in Fig. 1. Gelatin at 10% (w/v) concentration was poured in de-ionized distilled water that mixed with KH_2PO_4 (KH_2PO_4 is a main component of simulated body fluid (SBF) which is useful for bone formation due to the existence of orthophosphate group in its chemical structure) to which BaG nanoparticles were added in 10, 20, 30, 40 and 50 wt% and homogenized by a stirrer at 40 °C for 45 min. Then, five types of nanocomposites have been fabricated with five different percentages of BaG nanoparticles. These mixtures were poured into plastic Petri dishes (PS), to cast in layer form and frozen at −20 °C for 1 h.

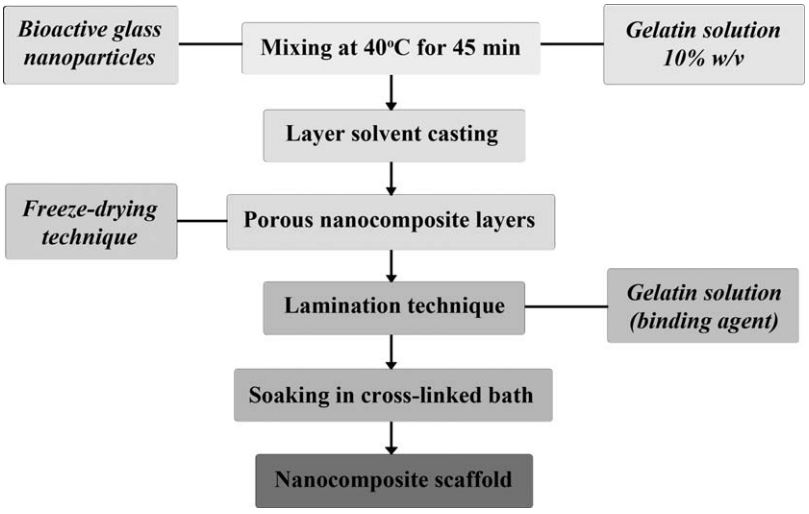

Fig. 1. The manufacturing process of hybrid nanocomposite scaffolds.

In the next step, the layers were moved to the freezer at −20 °C for 5 h and then it was moved to the freeze dryer at −57 °C and 0.05 mbar for 24 h in order to produce 3D porous structure through sublimation to form a gelatin network matrix on the pore walls and the surface of nanocomposite scaffolds. Then, composite layers were cut into proper sizes and laminated by applying a gelatin solution of 10% (w/v) as a binding agent.

Finally, to cross-link gelatin polymeric chains and to reduce biodegradation and enhance the biomechanical properties of the scaffolds for tissue repair, samples were soaked in a cross-linking bath with a GA solution of 1% (w/v) for 24 h, and samples were carefully washed after soaking in a GA solution.

2.4. Characterization

2.4.1. X-ray diffraction (XRD)

The resulting bioactive glass powder was analyzed by XRD with Siemens-Brucker D5000 diffractometer. This instrument works with voltage and current settings of 40 kV and 40 mA respectively and uses Cu-Ka radiation (1.540600 Å). For qualitative analysis, XRD diagrams were recorded in the interval $10^\circ \leq 2\theta \leq 50^\circ$ at scan speed of 2°/min being the step size 0.02° and the step time 1 s.

2.4.2. Transmission electron microscopy (TEM)

TEM studies were performed with the Philips CM120 operated at 100 kV. The morphology and size of the synthesized BaG nanoparticles assessed using TEM by dispersing in ethanol (0.1 g/10 mL) and ultrasound for 15 min. Finally, the samples were prepared by placing one drop of nanoparticles' dispersion on a carbon-coated grid.

2.4.3. N_2 adsorption analysis

The pore texture of BaG was analyzed with an automatic nitrogen adsorption pore size analyzer (Tristar 3000, Micromeritics) by N_2 adsorption method. The samples were degassed in vacuum at 150 °C for 18–20 h for the removal of moisture from the pores and analyzed with nitrogen adsorption. These analyses have provided the data of specific surface area, average pore size, and pore volume.

It is mentionable that pore size distribution was determined from a minimum of 20 points in the nitrogen desorption isotherm and calculated using the Barret, Joyner and Halenda model for cylindrical pores.

2.4.4. Fourier transform infrared spectroscopy (FTIR)

The functional groups of nanocomposite samples and the BaG nanoparticles were examined by FTIR with Bomem MB 100 spectrometer. For IR analysis, in first 1 mg of the powder samples were carefully mixed with 300 mg of KBr (infrared grade) and palletized under vacuum. Then the pellets were analyzed in the range of 400–4000 cm^{-1} at the scan speed of 23 scan/min with 4 cm^{-1} resolution.

2.4.5. Scanning electron microscopy (SEM) and energy dispersive X-ray (EDX) analyses

The morphology and microstructure of the synthesized BaG and nanocomposite samples and measurement of pore size were evaluated using SEM. The nanocomposite samples were coated with a thin layer of Gold (Au) by sputtering (EMITECH K450X, England) and then the morphology of them were observed on a scanning electron microscope (SEM-Philips XL30) that operated at the acceleration voltage of 15 kV.

Also, EDX (Rontec, Germany) directly connected to SEM was used to investigate semi-quantitatively chemical compositions.

2.4.6. Mechanical behavior

Mechanical behavior of the prepared nanocomposites was investigated by conducting compression strength test according to ASTM F 451-86. The cylindrical specimens were cut to 5 × 10 mm, and the thickness was measured with an electric digital caliper. *E* (Young Modulus) of the scaffolds were tested by Roel-Amstel (load cell: 25 kN; resolution: 1 N) with a drawing rate of 1 mm/min. Each test has been repeated five

times and the average amount and standard deviation (SD) of related parameters was determined.

2.5. Analytical methodology

2.5.1. Scaffolds density measurement

The apparent density of the samples (ρ_a) was measured by mercury pycnometry [34]. A sample of weight W_s was placed in a pycnometer, which was completely filled with mercury and weighted to obtain W_{sl}. ρ_a was calculated according to Eq. (1):

$$\rho_a = \frac{W}{W_l - W_{sl} + W_s} \times \rho_{Hg} \quad (1)$$

where W_l is the weight of the pycnometer filled with mercury, and ρ_{Hg} is the density of mercury (13.5 g/cm^3).

2.5.2. Pores sizes and porosity measurement

Pore volume (V_p) was calculated according to Eq. (2):

$$V_p = V_{sk} - V_{BG} - V_{Gel} = V_{sk} - \frac{W_{BG}}{\rho_{BG}} - \frac{W_{Gel}}{\rho_{Gel}} \quad (2)$$

where V_{sk} is the skeletal volume of the nanocomposite (cm^3), V_{BG} the actual volume of BaG (cm^3), V_{Gel} the actual volume of gelatin (cm^3), in addition V_{BG} and V_{Gel} measured with attention to the mass and the density of BaG and gelatin which were used in each sample. The density of BaG and gelatin are ($\rho = 2.7$) and ($\rho = 1.35$), respectively. So the calculation formula of porosity (%) is defined as follows Eq. (3):

$$\text{porosity } (\%) = \frac{V_p}{V_{sk}} \times 100 \quad (3)$$

It is calculated from the density of BaG, gelatin and the density of actual porous scaffolds sample produced. For the cylindrical samples which were cut to 5 × 10 mm, and the thickness was measured with an electric digital caliper, the total volume of each sample was 1.19625 cm^3.

By using SEM, the pore size of the cross-section, transverse section and the average pore diameter of the samples were observed.

2.6. Osteoblast cell culture

The *in vitro* biocompatibility of the nanocomposite scaffolds was tested using SaOS-2 cell line (human osteoblast-like cells) (National Cell Bank of Iran, Pasture Institute). The line was kept in continuous culture in Dulbecco's Modified Eagle Medium (DMEM) supplemented with 10% fetal bovine serum (FBS) and streptomycin/penicillin 100 U/mL (1%). The cells were detached with trypsin/EDTA before seeding on scaffolds.

For seeding, the cells were trypsinized, centrifuged and resuspended in complete culture medium. Aliquots of 200 μl containing 3×10^5 cells were then seeded on top of each scaffold sample pre-soaked in the medium. Cells/scaffold constructs were incubated for 4 days at 37 °C in a humidified atmosphere containing 5% CO_2. Then, the samples were washed twice with phosphate-buffered saline (PBS) and the cells were fixed. For fixation, samples were soaked in 2.5% GA for 1 h. Post-fixation was performed in 1% osmium tetroxide, and dehydration in a graded acetone series solution. Samples were then freeze-dried and kept dry using silica gel.

2.7. Statistical analysis

All experiments were performed in fifth replicate. The results were given as means ± standard error (SE). Statistical analysis was performed by using One-way ANOVA and Tukey test with significance reported when $P < 0.05$. Also for investigation of group normalizing, Kolmogorov–Smirnov test was used.

3. Result and discussions

3.1. XRD analysis

The XRD pattern of the synthesized BaG is presented in Fig. 2(a) The XRD pattern emphasized the predominant amorphous state of the internal disorder and glassy nature of this material feature of the sample and it is worth mentioning that the BaG does not show any crystalline states.

3.2. EDX analysis of BaG nanoparticles

Fig. 2(b) shows the EDX spectra of the synthesized BaG nanoparticle. The EDX spectrum shows the peaks of Si, P, Ca, and O. The presence of gold (Au) on the BaG surfaces was only related to the coating layer in SEM analysis. These results confirmed the nanoscale size and the composition of the synthesized BaG nanoparticles.

3.3. TEM observations of BaG nanoparticles

Due to TEM is a powerful tool for observing the morphology and particle sizes of nanoparticles, we used this test to estimate the BaG particle sizes and morphology. Fig. 3 shows the TEM micrograph of the synthesized BaG nanoparticles. The particles had nearly sphere shaped morphology and the particle size was less than 80 nm. The nanoparticles also showed uniformity in shape and size.

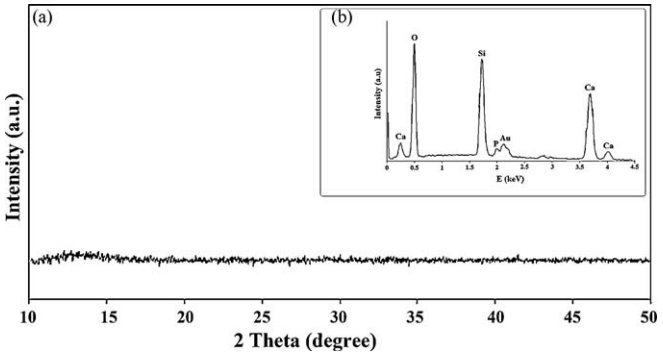

Fig. 2. (a) The XRD pattern of the BaG nanoparticles after stabilization at 700 °C and (b) The EDX pattern of the BaG nanoparticles.

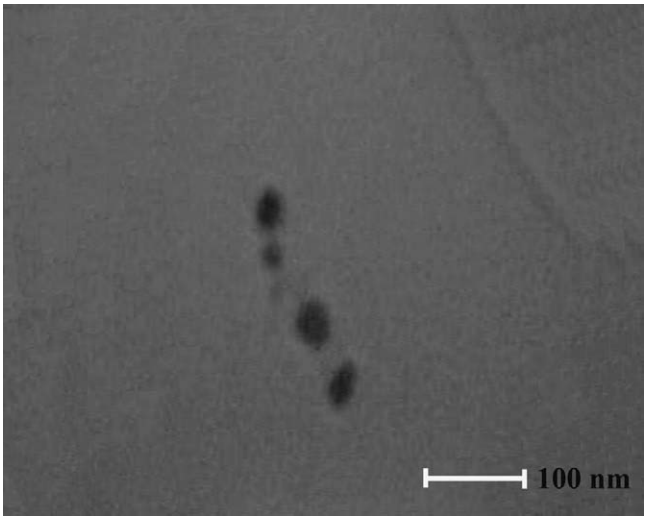

Fig. 3. The TEM micrograph of the BaG nanoparticles.

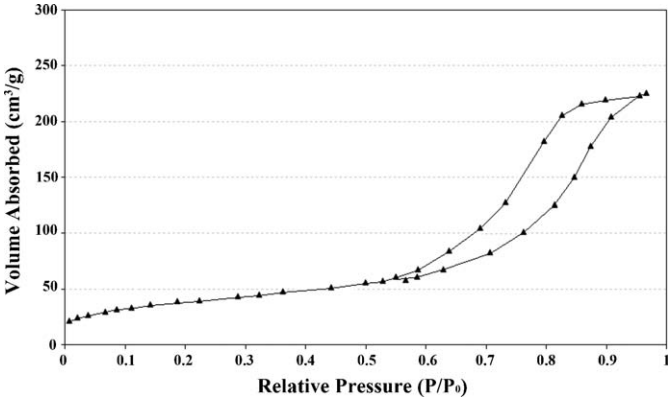

Fig. 4. The N_2 adsorption isotherm of the BaG nanoparticles.

3.4. Textural properties

The N_2 adsorption isotherm of the BaG is shown in Fig. 4 corresponds to the type IV isotherm of the Brunauer–Deming–Deming–Teller theory (BDDT) classification. From these results one can infer that the pores are in mesopores size range. The textural properties of this BaG are reported in Table 1.

This table shows that SiO_2–P_2O_5–CaO BaG has a nanoporous structure that provides controlled degradation and sites for cell attachment and protein adsorption.

3.5. FTIR analysis

Fig. 5 shows the FTIR spectra, in the 500–4000 cm^{-1} spectral range, of BaG and scraped material surfaces recorded after synthesis the nanocomposite scaffold.

The BaG nanoparticles exhibited five infrared bands located at: 609, 800, 930, 1070 and 1212 cm^{-1}. Among these bands,

Table 1
Textural properties of the bioactive glass.

BET surface area ($m^2\ g^{-1}$)	Pore volume ($cm^3\ g^{-1}$)	Pore size (nm)
137.9	0.37	15.4

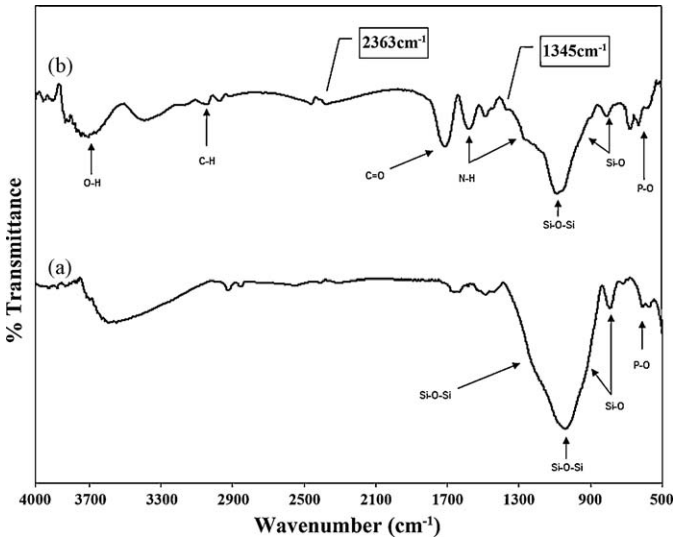

Fig. 5. The FTIR spectra of the synthesized BaG nanoparticles and the prepared nanocomposite scaffold cross-linked by GA.

those positioned at 800, 930, 1070 and 1212 cm^{-1} are related to the silicate network and respectively ascribed to the Si–O symmetric stretching of bridging oxygen atoms between tetrahedrons, Si–O stretching of non-bridging oxygen atoms, Si–O–Si symmetric stretching, and the LO mode of Si–O–Si asymmetric stretching. The band located at 609 cm^{-1} is attributed to the asymmetric vibration of PO_4^{3-} [35,36]. Similarly, Fig. 5 also represents the FTIR spectrum of the nanocomposite that exhibited a number of new characteristic spectral bands. The most characteristics of them were protein spectrums such as: N–H bending vibration at 1260 cm^{-1} for the amide III, N–H bending vibration at 1560 cm^{-1} for the amide II, C=O stretching vibration at 1670 cm^{-1} for the amide I, C–H bending vibration at 2952 cm^{-1} for the amide B and band at 3570 cm^{-1} indicate the presence of O–H groups, while the characteristic spectral bands for BaG was present in the spectrum for nanocomposite too [13].

It is worth mentioning that Fig. 5 also shows two peaks which are related to chemical bonds that has been formed due to the mixture of the BaG with gelatin and then cross-linking with GA. The first one at about 1345 cm^{-1} indicates formation of the chemical bond between carboxyl groups from gelatin and Ca^{2+} ions from the BaG that has been mentioned in former studies too for gelatin and hydroxyapatite [13,37,38]. The second bond at 2363 cm^{-1} appeared after cross-linking of gelatin with GA as mentioned former by Azami et al. [13]. GA reacts with gelatin chains observed in Scheme (4):

$$\mathrm{Gel{-}NH_2 + C_5H_8O_2 + NH_2{-}Gel} \rightarrow \mathrm{Gel{-}N{=}CH{-}C_3H_6{-}CH{=}N{-}Gel} \quad (4)$$

3.6. Chemical bonding reaction mechanism

The chemical bonding between the BaG nanoparticles and gelatin in the nanocomposites have three major steps, as shown in Fig. 6(a), is described in following:

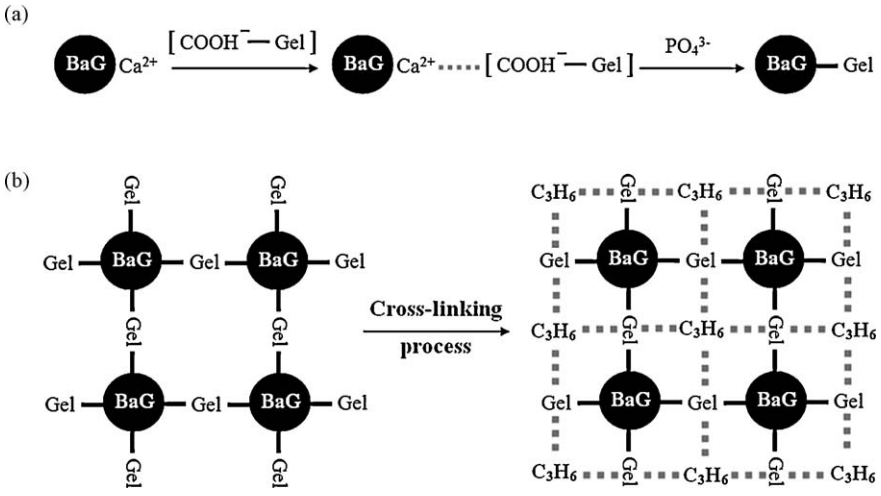

Fig. 6. (a) The mechanism of chemical bonding between the BaG nanoparticles and gelatin, and (b) The schematic of chemical bonding between gelatin chains and GA.

(1) A critical complex reaction between Ca^{2+} ions of BaG nanoparticles and gelatin molecules [39,40].
(2) The Ca^{2+} ions of complex with gelatin molecules assembled with PO_4^{3-} ions.
(3) The –COOH and $–NH_2$ groups in the gelatin molecule form chemical bonds with P–O and O–H groups of BaG nanoparticles, resulting in gelatin layer firmly attaching to the surface of BaG nanoparticles.

In addition, according to Minfang et al. [41], there are two main sources of stabilization which prevent the occurrence of the nanoparticles agglomeration in these kinds of systems, one is electrostatic stabilization, and the other is spatial stabilization. Electrostatic stabilization in this reaction system is mainly due to adsorption of Ca^{2+} ions on the surface of BaG nanoparticles. The adsorption would produce an electrical double layer. In other words, the ionization of carboxyl is enforced while that of amino is restrained, and the carboxyl ions of gelatin are consequently as counter ions in the electrical double layer. The spatial stabilization in this reaction system is mainly due to chemisorption of gelatin molecules on the BaG nanoparticles, and the gelatin formed a thick layer on the surface of BaG nanoparticles.

3.7. Cross-linking of the gelatin matrix structure

Because of the high degradation rate and low biomechanical stiffness of gelatin *in vivo*, cross-linking is necessary to reduce

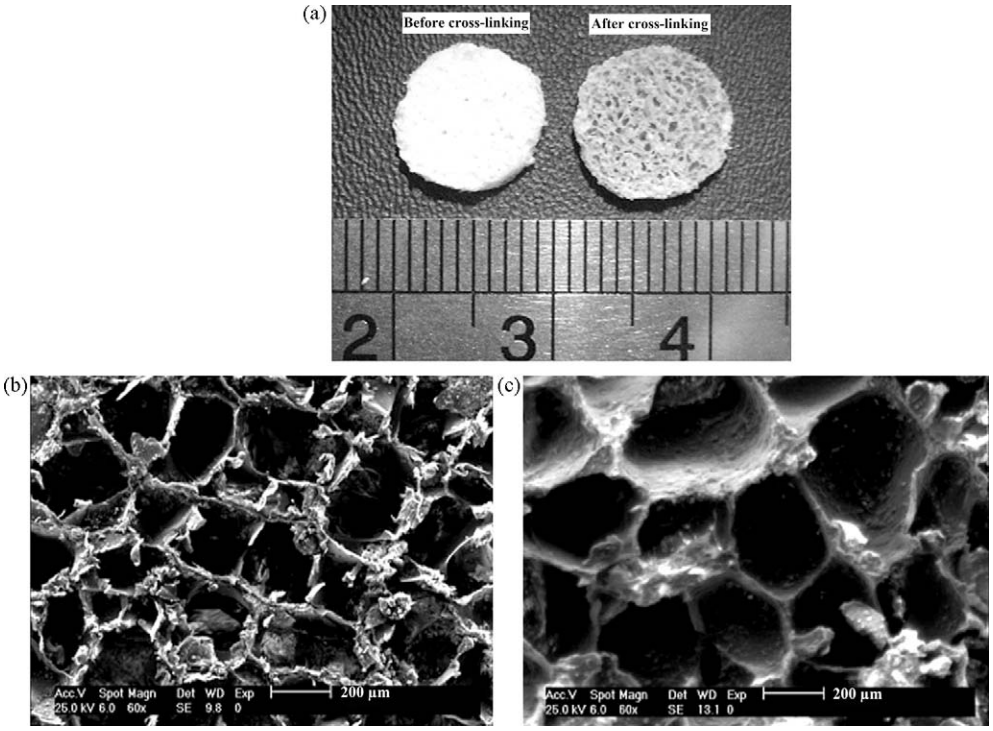

Fig. 7. (a) An overall view of the nanocomposites before and after cross-linking, (b) SEM micrograph of the nanocomposite (30% BaG) before cross-linking (top surface), and (c) SEM micrograph of the nanocomposite (30% BaG) after cross-linking (top surface).

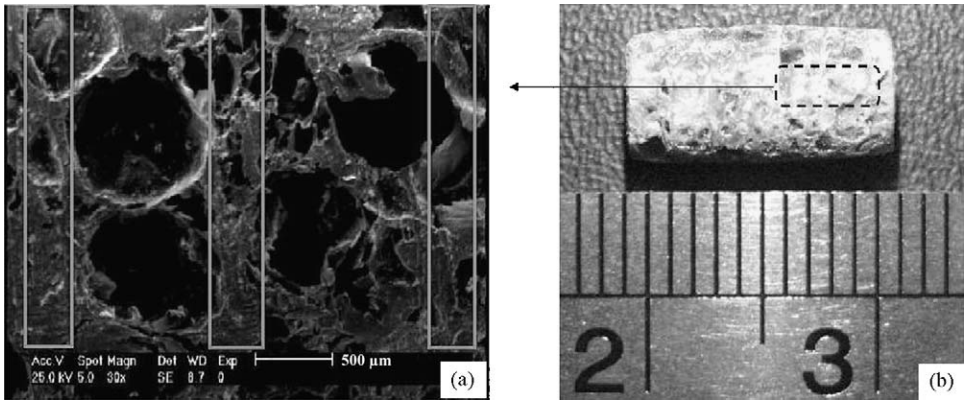

Fig. 8. (a) An overall view of the final nanocomposite scaffolds after lamination technique and (b) The SEM micrograph of final nanocomposite (lateral surface).

rate of biodegradation and enhance the biomechanical properties of the biomaterial for tissue repair.

In this study, GA ($OHCCH_2CH_2CH_2CHO$) was used as a cross-linking agent, which GA reacts with gelatin chains as observed in Fig. 6(c). Cross-linking processing occurred with C_3H_6 alkene bands. GA has two functional groups to be able to link with free amine groups of lysine or hydroxylysine amino acid residues of the polypeptide chains in gelatin. All available free amine groups of gelatin react with the aldehyde groups of GA to form Schiff bases within 5 min and then a large variety of subsequent reactions are involved in the cross-linking of the material [42,43].

The gelatin matrix structure after cross-linking which shows in Fig. 7(c) became denser and more ordered, compared with noncross-linked gelatin structure that shown in Fig. 7(b) it was highly porous with parallel aligned and inter-connected pores. The pores were close to square with the size ranged from 200 to 500 μm which is desirable for bone cell growth.

Fig. 8 also shows fine adhesion beyond composite layers along their interfaces to each other which approve that gelatin solution is able to acts as a good binder for nanocomposite layers.

It is mentionable that the biomechanical properties of gelatin material before and after cross-linking were also analyzed which shows that cross-linking could increase biomechanical property pretty well. GA cross-linkage significantly increased the rupture strength of wet matrices compared with noncross-linked controls, which will greatly contribute to future, *in vivo*, tissue implantation.

Also, as it can be observed in Fig. 9 the BaG nanoparticles are dispersed in cross-linked gelatin matrix.

3.8. Mechanical properties

Table 2 gives the data obtained from mechanical compressive tests of nanocomposite samples and compares them with spongy and compact bone. Generally, elastic modulus (E) enhanced with increasing the percentage of BaG nanopowder. E values varied from 50 MPa to about 80 MPa. It is worth mentioning that the density (ρ) and the porosity percentages are in the range of natural spongy bone and also, comparison between specific elastic modulus (E/q) indicates that properties of prepared nanocomposites are very close to natural spongy bone.

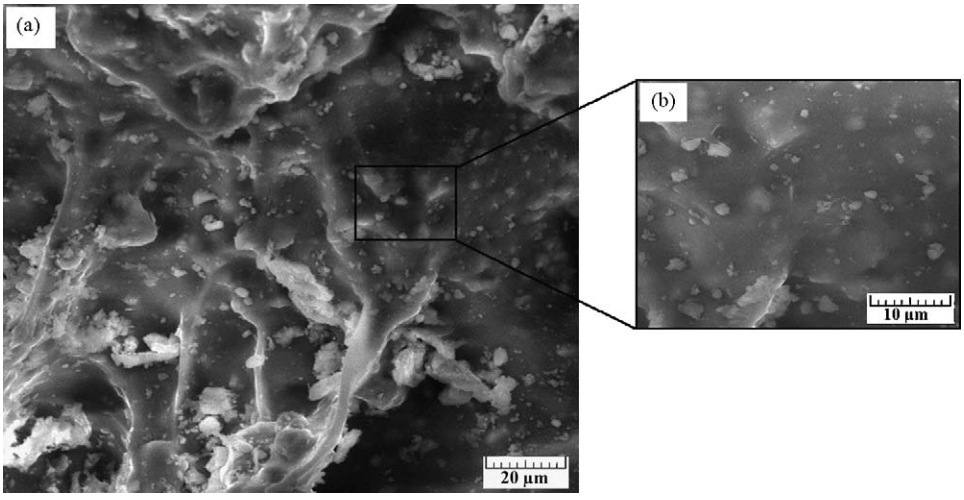

Fig. 9. The SEM micrographs of the nanocomposite sample showing the dispersion of BaG nanoparticles through the cross-linked gelatin matrix (a) low and (b) high magnification.

Table 2
Mechanical compressive tests of nanocomposite samples, spongy and compact bone.

Sample	E (MPa)	ρ (g/cm^3)	E/ρ	Pore volume (cm^3)	Porosity (%)
Compact bone	3–30 × 10^3	1.8–2	7.78–10 × 10^3	–	5–30
Spongy bone	20–500	0.14–1.2	500	–	30–90
Nanocomposite (10% BaG)	51 ± 1.8	0.192 ± 0.005	275 ± 8	0.169	86 ± 1.1
Nanocomposite (20% BaG)	58 ± 2.1	0.265 ± 0.014	231 ± 4	0.159	81 ± 0.8
Nanocomposite (30% BaG)	64 ± 1.3	0.336 ± 0.001	200.5 ± 4.5	0.152	77 ± 1.2
Nanocomposite (40% BaG)	72 ± 1.7	0.424 ± 0.013	173.5 ± 3.5	0.145	74 ± 1
Nanocomposite (50% BaG)	78 ± 1.2	0.491 ± 0.005	160 ± 2	0.140	72 ± 0.66

In addition, by using SEM, the average pore diameter of the nanocomposite samples was observed. Fig. 10 related to the pore size (μm) vs bioactive glass (%) showed that the pore sizes were in the range of 200–500 μm.

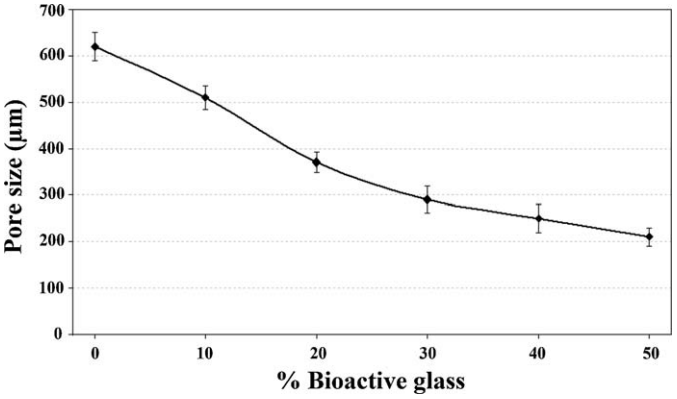

Fig. 10. The average pore diameter of the nanocomposite scaffolds.

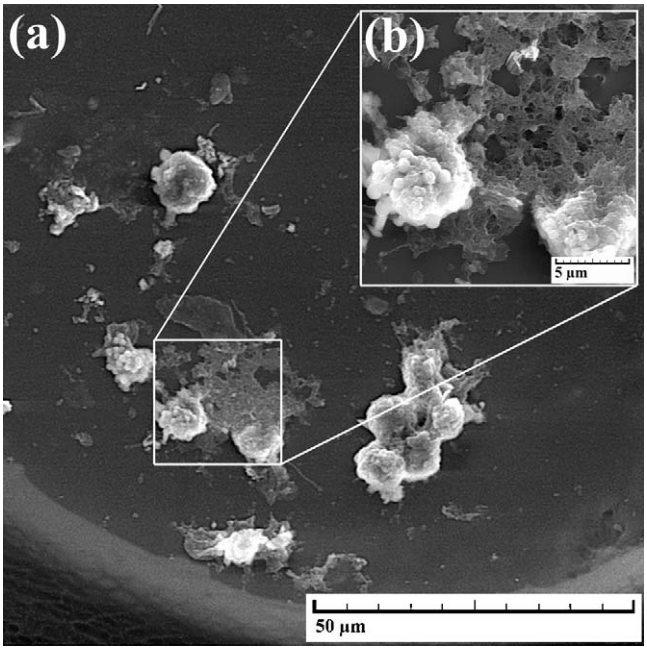

Fig. 11. The SEM micrographs of the osteoblastic cells grown on the nanocomposite scaffolds after culturing for 3 days (a) low and (b) high magnification.

3.9. Biocompatibilty evaluation

The SEM micrographs of the SaOS-2 cell line (human osteoblast-like cells) cultured on bioactive scaffolds are shown in Fig. 11(a) and (b) showed well-spread cells on the scaffolds with numerous lamellipodia and filopodia, an indication of good attachment and penetration to the pores of scaffolds. The cells actively secrete extracellular matrix (ECM), which can be observed on both cells and scaffold surfaces. ECM gave an unsmooth appearance to the cells. The cells left traces of ECM along their migration path. Wide distribution of these traces on the scaffold surfaces is an indication of good cellular migration and osteoconductivity of the scaffolds. The continuous increase in cell aggregation on the bioactive scaffolds during the 3 days incubation indicated the ability of the scaffolds to support cell growth.

4. Conclusions

In summary, the gelatin/BaG nanoparticles nanocomposites were prepared by layer solvent casting combined with freeze-drying and lamination techniques as a bioactive nanocomposite scaffold. The interest of processing bone tissue-engineered scaffolds with both highly porous structure and desired mechanical strength drives us to focus on preparing scaffolds using the materials compounding synthetic gelatin with BaG nanoparticles. The results have demonstrated that these nanocomposite scaffolds were 3D porous and that the Young Modulus of the scaffolds was comparative to the natural spongy bone. Also, applying BaG/gelatin nanocomposite scaffolds is notable from two points of view including improved cell culture response and higher reinforcing quality of BaG nanoparticles, with increasing amount of reinforcing nanoparticles. Also, the surface area of reaction zone between particles and matrix will dramatically increase and thus improve the mechanical properties of overall nanocomposite. This feature will be intensified particularly when a kind of chemical bonding form between matrix and reinforcing particles. Finally, SEM micrographs of osteoblast-like cells obtained after culture of these cells on the scaffolds showed that osteoblasts demonstrate adhesion, migration and penetration to the pores of scaffold. Therefore, wide distribution of these traces on the scaffold surfaces could be an indication of good cellular migration and osteoconductivity of these bioactive scaffolds.

Acknowledgement

The authors would like to thank many colleagues, PhD students and collaborators who have made a vast contribution to this area of research. We are also grateful for support of this research by Amirkabir University of Technology.

References

[1] D.W. Hutmacher, Scaffolds in tissue engineering bone and cartilage, Biomaterials 21 (2000) 2529–2531.
[2] R.A. Quirk, M.C. Davies, S.J.B. Tendler, K.M. Shakesheff, Surface engineering of poly(lactic acid) by entrapment of modifying species, Macromolecules 33 (2000) 158–160.
[3] A.S. Goldstein, T.M. Juarez, C.D. Helmke, M.C. Gustin, A.G. Mikos, Effect of convection on osteoblastic cell growth and function in biodegradable polymer foam scaffolds, Biomaterials 22 (2001) 1279–1288.
[4] L.D. Shea, D. Wang, R.T. Franceschi, D.J. Mooney, Engineered bone development from a pre-osteoblast cell line on three-dimensional scaffolds, Tissue Eng. 6 (2000) 605–617.
[5] V. Maquet, A.R. Boccaccini, L. Pravataa, I. Notingher, R. Jerome, Porous poly(a-hydroxyacid)/Bioglass® composite scaffolds for bone tissue engineering. I: Preparation and in vitro characterization, Biomaterials 25 (2004) 4185–4194.
[6] J.R. Jones, New trends in bioactive scaffolds: the importance of nanostructure, J. Eur. Ceram. Soc. 29 (2009) 1275–1281.
[7] X. Su, K. Sun, F.Z. Cui, W.J. Landis, Organization of apatite crystals in human woven bone, Bone 32 (2003) 150–162.
[8] E.L. Hedberg, C.K. Shih, J.J. Lemoine, M.D. Timmer, M.A.K. Liebschner, J.A. Jansen, A.G. Mikos, *In vitro* degradation of porous poly (propylene fumarate)/poly(DL-lactic-co-glycolic acid) composite scaffolds, Biomaterials 26 (2005) 3215–3225.
[9] S.H. Rhee, S.J. Lee, Effect of acidic degradation products of poly(lactic-co-glycolic)acid on the apatite-forming ability of poly(lacticco-glycolic)acid-siloxane nanohybrid material, J. Biomed. Mater. Res. 83A (2007) 799–805.
[10] H.A. ElBatal, M.A. Azooz, E.M.A. Khalil, A. Soltan Monem, Y.M. Hamdy, Characterization of some bioglass–ceramics, Mater. Chem. Phys. 80 (2003) 599–609.
[11] H. Boedtker, P. Doty, A study of gelatin molecules aggregates and gels, J. Phys. Chem. 58 (1954) 968–983.
[12] X. Liu, L.A. Smith, J. Hu, P.X. Ma, Biomimetic nanofibrous gelatin/apatite composite scaffolds for bone tissue engineering, Biomaterials 30 (2009) 2252–2258.
[13] M. Azami, F. Moztarzadeh, M. Tahriri, Preparation, characterization and mechanical properties of controlled porous gelatin/hydroxyapatite nanocomposite through layer solvent casting combined with freeze-drying and lamination techniques, J. Porous Mater. (2009), doi:10.1007/s10934-009-9294-3.
[14] M.P. Lutolf, J.A. Hubbell, Synthetic biomaterials as instructive extracellular microenvironments for morphogenesis in tissue engineering, Nat. Biotechnol. 23 (2005) 47–55.
[15] C.T. Lawrencin, S.F. El Amin, S.E. Ibim, D.A. Willoughby, M. Attavia, H.R. Allcock, A.A. Ambrosio, A highly porous 3-dimensional polyphosphazene polymer matrix for skeletal tissue regeneration, J. Biomed. Mater. Res. 30 (1996) 133–138.
[16] X. Liu, W. Huang, H. Fu, A. Yao, D. Wang, H. Pan, W.W. Lu, Bioactive borosilicate glass scaffolds: *in vitro* degradation and bioactivity behaviors, J. Mater. Sci. Mater. Med. 20 (2009) 365–372.
[17] M.C. Chang, T. Ikoma, M. Kikuchi, J. Tanaka, Preparation of a porous hydroxyapatite/collagen nanocomposite using glutaraldehyde as a crosslinkage agent, J. Mater. Sci. Lett. 20 (2001) 1109–1201.
[18] Z.M. Huang, Y.Z. Zhang, S. Ramakrishna, C.T. Lim, Electrospinning and mechanical characterization of gelatin nanofibers, Polymer 45 (2004) 5361–5368.
[19] H.W. Kim, J.H. Song, H.E. Kim, Nanofiber generation of gelatin–hydroxyapatite biomimetics for guided tissue regeneration, Adv. Funct. Mater. 15 (2005) 1988–1994.
[20] H. Yuan, J.D. De Bruijn, X. Zhang, C.A. Van Bitterswijk, K. De Groot, Factors affecting the structure and properties of bioactive foam scaffolds for tissue engineering, J. Biomed. Mater. Res. 58 (2008) 270–276.
[21] J.M. Taboas, R.D. Maddox, P.H. Krebsbach, S.J. Hollister, Indirect solid free form fabrication of local and global porous, biomimetic and composite 3D polymer-ceramic scaffolds, Biomaterials 24 (2003) 181–194.
[22] J.R Jones, S. Ahir, L.L. Hench, Large-scale production of 3D bioactive glass macroporous, J. Sol–Gel Sci. Technol. 29 (2004) 179–188.
[23] K.G. Carrasquillo, A.M. Stanley, J.C. Aponte-Carro, P. De Jé sus, H.R. Costantino, C.J. Bosques, Non-aqueous encapsulation of excipient-stabilized spray freeze dried BSA into poly(lactide-co-glycolide) microspheres results in release of native protein, J. Control Release 76 (2001) 199–208.
[24] H. Fu, Q. Fu, N. Zhou, W. Huang, M.N. Rahaman, D. Wang, X. Liu, *In vitro* evaluation of borate-based bioactive glass scaffolds prepared by a polymer foam replication method, Mater. Sci. Eng. C 29 (2009) 2079–2312.
[25] M. Wang, Composite Scaffolds for bone tissue engineering, Am. J. Biochem. Biotechnol. 2 (2006) 80–84.
[26] L.L. Hench, J. Wilson, Introduction to Bioceramics, World Scientific, Singapore, 1993.
[27] S.H. Li, J.R. De Wijn, P. Layrolle, K. de Groot, Synthesis of macroporous hydroxyapatite scaffolds for tissue engineering, J. Biomed. Mater. Res. 61 (2002) 109–120.
[28] L.L. Hench, J. Wilson, Clinical Perfomance of Skeletal Prostheses, Chapman and Hall, London, 1996.
[29] W. Cao, L.L. Hench, Bioactive materials, Ceram. Int. 22 (1996) 493.
[30] M. Navarro, M.P. Ginebra, J.A. Planell, Cellular response to calcium phosphate glasses with controlled solubility, J. Biomed. Mater. Res. 67A (2003) 1009.
[31] J.M. Polak, L.L. Hench, P. Kemp, Future strategies for tissue and organ replacement, in: L.L. Hench, J.R. Jones, P. Sepulveda (Eds.), Bioactive Materials for Tissue Engineering Scaffolds, Imperial College Press, London, 2002, pp. 1–22.
[32] L.L. Hench, The challenge of orthopaedic materials, Curr. Orthop. 14 (2000) 7–15.
[33] L.L. Hench, J.K. West, Biological applications of bioactive glasses, Life Chem. Rep. 13 (1996) 187–241.
[34] V. Maquet, A.R. Boccaccini, L. Pravata, I. Notingher, R. Jerome, Preparation, characterisation and *in vitro* degradation of bioresorbable and bioactive composites based on bioglass-filled polylactide foams, J. Biomed. Mater. Res. 66A (2003) 335–346.
[35] M. Mami, A. Lucas-Girot, H. Oudadesse, R. Dorbez-Sridi, F. Mezahi, E. Dietrich, Investigation of the surface reactivity of a sol gel derived glass in the ternary system SiO_2–CaO–P_2O_5, Appl. Surf. Sci. 254 (2008) 7386–7393.
[36] J.J. Vidueau, V. Dupius, Phosphates biomaterials, Eur. J. Solid State Inorg. Chem. 28 (1991) 303–343.
[37] J. Tian, J. Tian, Tian preparation of porous hydroxyapatite, J. Mater. Sci. 36 (2001) 3061–3066.
[38] U.C. Chang, C. Ko, W.H. Douglas, Preparation of hydroxyapatite-gelatin nanocomposite, Biomaterials 24 (2003) 2853–2862.
[39] S. Teng, J. Shi, B. Peng, L. ChenF, The effect of alginate addition on the structure and morphology of hydroxyapatite/gelatin Nanocomposites, Compos. Sci. Technol. 66 (2006) 1532–1538.
[40] M.C. Chang, C.C. Ko, W.H. Douglas, Conformational change of hydroxyapatite-gelatin nanocomposite by glutaraldehyde, Biomaterials 24 (2003) 3087–3094.
[41] C. Minfang, T. Junjun, L. Yuying, L. Debao, Preparation of gelatin coated hydroxyapatite nanorods and the stability of its aqueous colloidal, Appl. Surf. Sci. 254 (2008) 2730–2735.
[42] L.H.H. Olde Damink, P.J. Dijkstra, M.J.A. Van Luyn, P.B. Van Wachem, Glutaraldehyde as a crosslinking agent for collagen-based biomaterials, J. Mater. Sci. Mater. Med. 6 (1995) 460–472.
[43] S. Matsuda, H. Iwata, N. Se, Y. Ikata, Bioadhesion gelatin films crosslinked with glutaraldehyde, J. Biomed. Mater. Res. 45 (1999) 20–27.